Transient Performance and Loss Analysis in Solid Wound Rotor Pulsed Power Generators

Kent R. Davey, IEEE Fellow

***Abstract*—High rotation speed is the key to enhanced power density in rotating machines. High speed, shock, and construction considerations argue for solid rotors. However, output transient voltage requirements cause concern that changes in the field current will not be registered quickly in the stator. Different techniques are considered for estimating the machine time constant, including an analytic solution of a smooth air gap machine, and a transfer relation solution based on time harmonic solutions. An empirical solution and an equivalent surface current approach are discussed for predicting the loss in the rotor. These solutions compare favorably to rotational transient finite element solutions.**

***Index Terms*—harmonic, power dissipation, rotating machine, transfer relation, transient, wound rotor**

I. Introduction and Motivation

CONSIDERABLE research attention is being given to the design of pulsed power generators for special magnetic field experiments [1], plasma ion implantation [2], rail guns [3], X ray simulators [4], and electromagnetic launchers [5][6]. The unique feature of pulsed power machines is that they function in a transient regime. High power density and short transient reaction times are important for many of these applications, and the natural choice is a brushless wound rotor synchronous machine. High power density translates to high rotation speed. Reliable operation in a high shock environment suggests a solid rotor rather than laminated construction. Certainly, mechanical and assembly complications are eased considerably over a laminated rotor, and the solid rotor eddy currents suppress spikes in pulsed charging circuits. The pros and cons are quite complex in this decision. This paper is not concerned about answering that question definitively, but rather with the analysis required to make an intelligent decision for its selection. An informed decision requires information about the time constant relating voltage changes on the exciter to voltage on the stator, and losses induced in the rotor.

For an application driving this research, it is important to change the output voltage and power to 100-400 ms. Will the eddy currents in the solid rotor allow this rapid transient performance? Will the losses in the rotor be acceptable? Does a hybrid rotor make for a suitable compromise, i.e., one with very large laminations? Are there reasonable techniques for working this problem, apart from a discrete time-step full transient solver approach?

Both analytic solution and one based on time harmonic solutions are presented for estimating the transient response. These are compared to a full transient finite element solution. Then an empirical solution and an equivalent surface current solution are presented for estimating the power dissipation in the rotor. There are five reasons why these approaches merit attention in lieu of a full transient finite element approach.

1. A transient finite element solver requires considerable computation time and quickly becomes intractable in three dimensions when macro-laminations are introduced.
2. Although transient field solvers are available through many commercial sources, these codes are expensive, and not readily available to many researchers.
3. Analytic solutions are parametrically unbeatable, i.e., the effect of material and dimensioned parameter change is immediate and instructive.
4. A handful of time harmonic solutions can be obtained with most numerical solvers in three dimensions in two to three days, a fraction of that required for a full transient solver. Among the complications presented to the transient solver is generally the requirement of remeshing at least a portion of the air gap at every step.
5. Approximations to the time constant or the loss are quite valuable at the early design stage.

II. Time Constant Analysis

A. Quantifying the Problem

The device under consideration is a solid wound rotor brushless synchronous generator, such as that in Fig. 1, with the requirement that the current in the stator winding be tightly controlled between 100 and 400 ms. A quick way to index the severity of the problem is to examine the two dimensional magnetic field reduction when the exciter operates at a frequency equal to the reciprocal of the desired reaction time, which in this case is 0.1 s. As shown in Fig. 2, the radial B field along the middle of the air gap when the rotor is solid is 41% of that produced when the rotor is fully laminated. The trace annotated “deep rotor slot” was computed to address the question “How much additional magnetomotive force (MMF) would be required on the rotor

Manuscript received May 18, 2005.

K. R. Davey is with the Center for Electromechanics at the University of Texas, 10100 Burnet Rd., Bldg. EME 133, Austin, TX 78758. (phone: 512-232-1603; fax: 512-471-0781; e-mail: k.davey@mail.utexas.edu).

to compensate for the suppression by the induced rotor eddy currents?" The answer is about three fold more at 10 Hz.

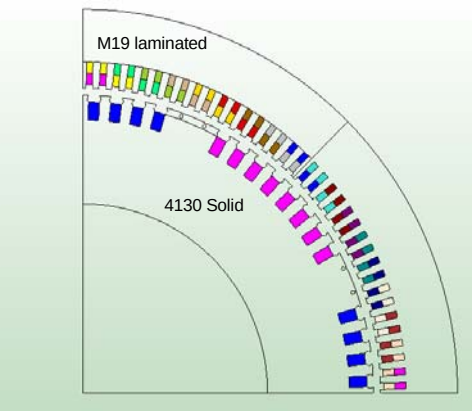

Fig. 1. Cross-section of a wound rotor generator with a solid 4130 rotor and M-19 stator.

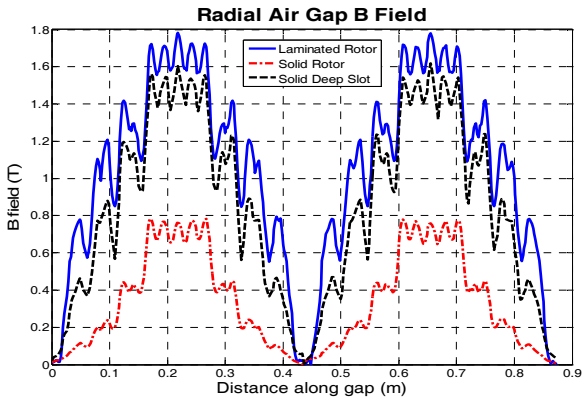

Fig. 2. Air gap B field reduction for laminated and solid rotors.

B. Estimating the Generator's Time Constant using Time Harmonic Solutions

The concept of using time harmonic solutions in transient field analysis was first presented by this author in [7]. It is applied and further developed in the problem under study. The field time constant is a number that varies considerably over the excitation range. The ability to get flux from the rotor to the stator improves as the material is pushed harder into saturation. The problem's characteristic time constant must be bound within a range of field excitation. Consider first describing the generator's time constant near its rated pulsed peak field current of 18 MA/m^2. Compute both the flux linking the field winding and the flux penetrating into the armature at each time. The field circuit current I_0 and voltage V are linked by the coil's flux linkage λ and its resistance R as

$$V = \frac{d\lambda}{dt} + RI_0 . \qquad (1)$$

The field coil inductance L is simply λ/I. Assuming a 50% fill factor on the field slot cross-section, and accounting for the end turn effects on resistance, the L/R time constant is shown in Fig. 3. The effect of the induced eddy currents in the solid rotor is reflected by the nonlinear drop in inductance with increasing frequency. The inductance drops both with increasing frequency and increasing current. The induced solid rotor current opposes field changes, resulting in a time delay required to get flux from the field winding to the stator.

Is there a way to estimate this delay with the material frozen in its permeability state during maximum excitation? Examining the generator performance at full field load for various frequencies allows a prediction of transient performance expectations near peak excitation. The saturation state of both the rotor and the stator is affected by the magnitude of the induced eddy current; the problem is quite non-linear. Laplace transforms are linear tools for time transient problems. With that proviso comes the recognition that they can still be used to give an approximation to transient performance within certain excitation regimes.

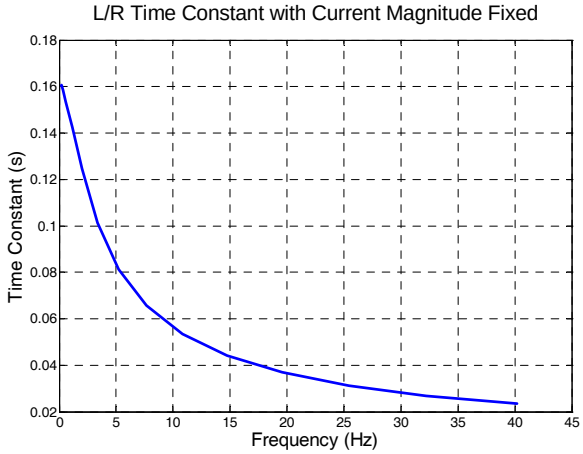

Fig. 3. Characteristic time constant versus frequency under constant excitation.

The inverse problem of determining the current I that would flow if the voltage were fixed and the material state close to what is expected at peak current I_0 can be estimated as

$$I = \frac{V}{\frac{1}{I_0}\frac{d\lambda}{dt} + R} . \qquad (2)$$

The link between voltage and current serves as a means for estimating the transfer relation between the voltage and current, analogous to how it would be constructed from a Bode plot. Fig. 4 shows the relation between the voltage and current when computed using a two dimensional code. The following pole-zero combinations were attempted in building a transfer relation linking voltage and current. Note that I_0 is the current at infinity.

$$I = \frac{p_1 \cdot I_0}{(j\omega + p_1)} \qquad (3)$$

$$I = I_0 \frac{\frac{p_1 \cdot p_2}{z_1} \cdot (j\omega + z_1)}{(j\omega + p_1)(j\omega + p_2)} \tag{4}$$

$$I = I_0 \frac{\frac{p_1 \cdot p_2 \cdot p_3}{z_1 \cdot z_2} \cdot (j\omega + z_1)(j\omega + z_2)}{(j\omega + p_1)(j\omega + p_2)(j\omega + p_3)} \tag{5}$$

A subspace trust region search algorithm based on the interior-reflective Newton method was employed to find the best pole–zero locations [8][9]. These poles are found by minimizing the absolute value of the difference between the computed current and the transfer equivalent. For the single pole approximation, one minimizes

$$\left\{ |I| - \left| \frac{p_1 \cdot I_0}{(j\omega + p_1)} \right| \right\}^2 . \tag{6}$$

The pole locations for these three representations are respectively, 6.77, [4.5, 152.3], and [4.35, 232, 854]. The location of the secondary poles makes it clear that the secondary effects die out rapidly.

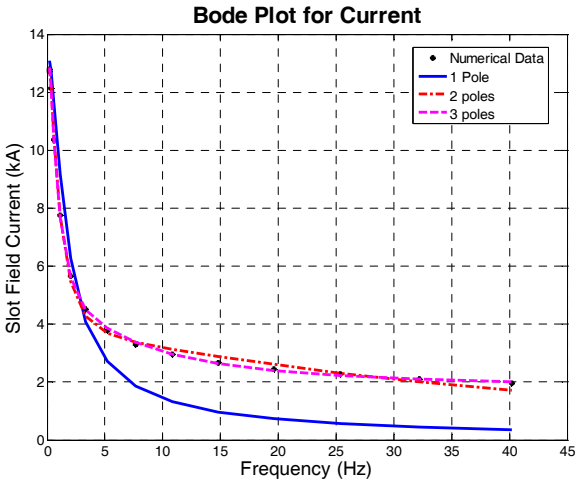

Fig. 4. Bode relation between field voltage and current as a function of frequency.

C. Time Transient Current Response

How are the transfer relations used to approximate the temporal transients? Each of the expressions in (3) through (5) should be replaced with their Laplace transform equivalent.

$$I = \frac{p_1 \cdot I_0}{(s + p_1)} \tag{7}$$

$$I = I_0 \frac{\frac{p_1 \cdot p_2}{z_1} \cdot (s + z_1)}{(s + p_1)(s + p_2)} \tag{8}$$

$$I = I_0 \frac{\frac{p_1 \cdot p_2 \cdot p_3}{z_1 \cdot z_2} \cdot (s + z_1)(s + z_2)}{(s + p_1)(s + p_2)(s + p_3)} \tag{9}$$

To predict the current expected when a step voltage source is used for the source, I_0 should be replaced with I_0/s and an inverse Laplace transform performed. Inverting *1/s* times equations (7) through (9) yields the step response

$$I(t) = 2 I_0 e^{-\left(\frac{1}{2} p_1 t\right)} \sinh\left(\frac{1}{2} p_1 t\right), \tag{10}$$

$$I = I_0 \left(1 - \frac{p_1 (z_1 - p_2) e^{-p_2 t} + p_2 (p_1 - z_1) e^{-p_1 t}}{z_1 (p_1 - p_2)} \right), \tag{11}$$

$$I = I_0 \left(1 - \frac{p_1 p_2 (z_2 - p_3)(z_1 - p_3) e^{-p_3 t}}{z_1 z_2 (p_1 - p_3)(p_2 - p_3)} - \frac{p_3 p_2 (z_2 - p_1)(z_1 - p_1) e^{-p_1 t}}{z_1 z_2 (p_1 - p_3)(p_1 - p_2)} - \frac{p_1 p_3 (z_2 - p_2)(z_1 - p_2) e^{-p_2 t}}{z_1 z_2 (p_1 - p_2)(p_2 - p_3)} \right) \tag{12}$$

Fig. 5 shows the normalized field current resulting from a step change in voltage. The first three traces are those resulting from the complex pole fit.

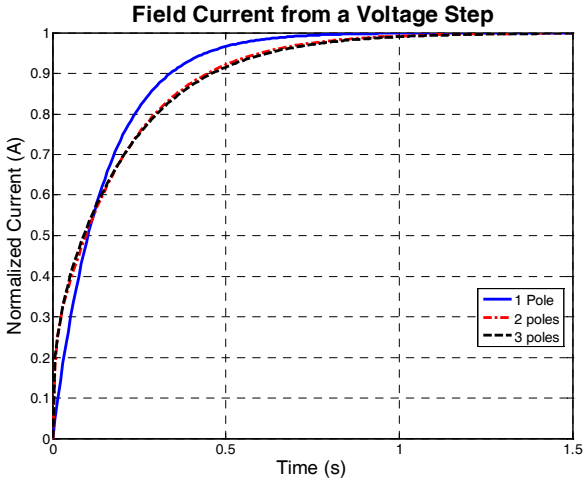

Fig. 5. Current response to a step voltage placed across the field coils.

The closeness of these approximations and the convergence of the 2nd and 3rd pole approximation make it clear that a higher order approximation is unnecessary. This is even clearer for flux linkage, where the important first pole for the 1 pole, 2 pole, and 3 pole representations are respectively 4.349, 4.335, and 4.337.

1) Flux Linkage with the Stator

The primary concern in this study is how long it will take for a step voltage change on the field winding to impact the flux being linked by the stator. If the procedure outlined in the previous section is repeated for the flux linking the two coils annotated in Fig. 6, a time response of the flux linking the stator can be estimated.

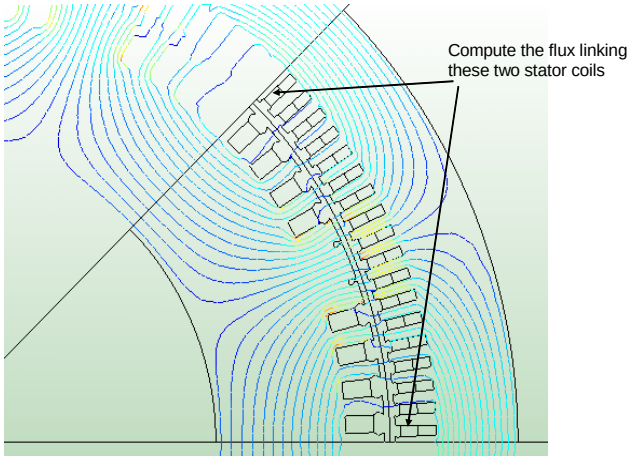

Fig. 6. Flux linking the stator coils is the primary interest.

Based on the information learned from Fig. 5, a two pole approximation will be used to predict the step response of flux linking the stator in response to a step voltage on the field winding. This time is longer than that for the current. Whereas the single pole location for current is 13.6 for the current, it is 5.2 for the flux linkage. There are two reasons that the three dimensional time response in Fig. 7 is shorter than the two dimensional estimate. In three dimensions the induced current is forced to make the bends at the ends. It is also forced to take a longer path to get around the rotor field slots that block the azimuthal current. Both facts increase the resistance, and thus lower the effective time constant.

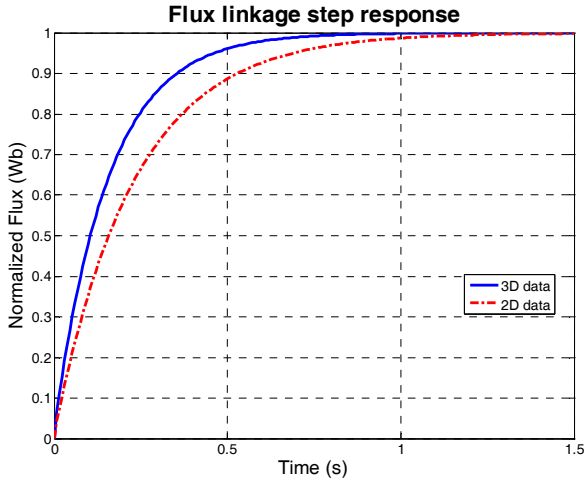

Fig. 7. Solid rotor flux linkage time response to a step voltage change when the field current is close to its rated peak value.

The step response for the low excitation, high permeability case is predicted in three dimensions both for a single section rotor, and for the four section rotor shown in Fig. 8. The fact that the full model has a slightly lower time response in Fig. 9 is due to numerical inaccuracy. The results are essentially identical, and show that a considerable reduction in lamination thickness is required before a worthwhile reduction in the transient constant is witnessed.

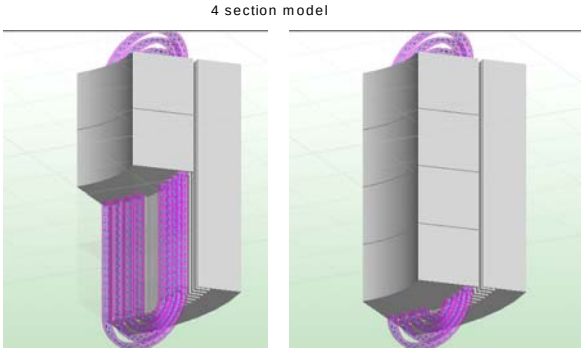

Fig. 8. Four section three dimensional model.

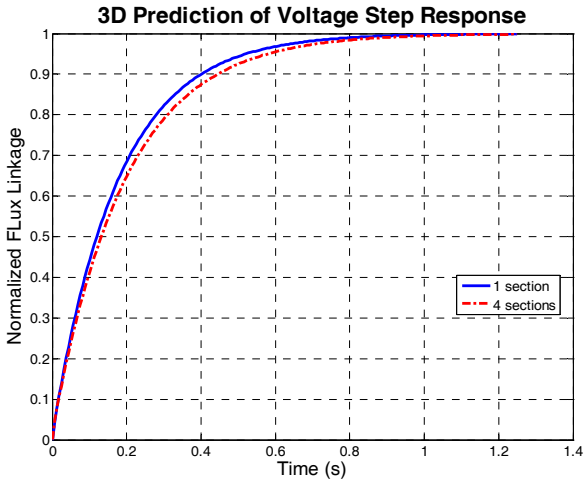

Fig. 9. Time response comparison for a one section and a full section model.

III. Analytical Solution

Consider the 1/8th model smooth bore rotor – stator shown in Fig. 10.

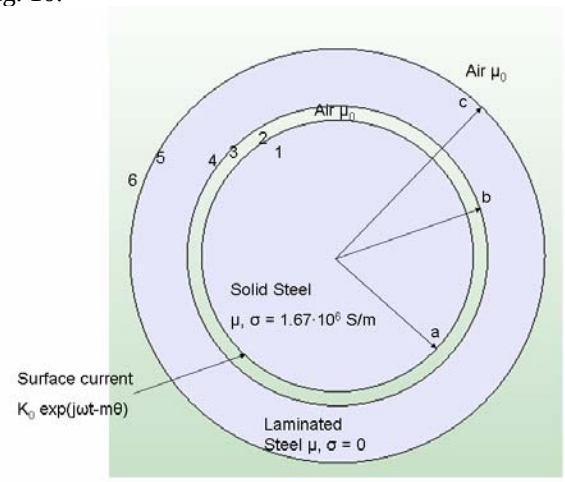

Fig. 10. Geometry used for analytical confirmation.

A surface current on surface 2 is used to excite the rotor having the phasor representation

$$K_f = K_0 e^{j(\omega t - 4\theta)}. \qquad (13)$$

In each region the vector potential which has only a z component must satisfy the equation

$$\frac{1}{\mu\sigma}\nabla^2 A = \frac{\partial A}{\partial t}. \tag{14}$$

Using the phasor representation $A = \tilde{A}e^{j(\omega t - m\theta)}$, (14) can be written as

$$\frac{d^2\tilde{A}}{dr^2} + \frac{1}{r}\frac{d\tilde{A}}{dr} - \left(\gamma^2 + \frac{m^2}{r^2}\right)\tilde{A} = 0. \tag{15}$$

The solutions for this equation in any region with inner radius β and outer radius α is

$$\begin{aligned}\tilde{A} = \tilde{A}^{\alpha}\frac{\left[H_m(j\gamma\beta)J_m(j\gamma r) - J_m(j\gamma\beta)H_m(j\gamma r)\right]}{\left[H_m(j\gamma\beta)J_m(j\gamma\alpha) - J_m(j\gamma\beta)H_m(j\gamma\alpha)\right]} \\ + \tilde{A}^{\beta}\frac{\left[H_m(j\gamma\alpha)J_m(j\gamma r) - J_m(j\gamma\alpha)H_m(j\gamma r)\right]}{\left[H_m(j\gamma\alpha)J_m(j\gamma\beta) - J_m(j\gamma\alpha)H_m(j\gamma\beta)\right]}\end{aligned} \tag{16}$$

The azimuthal *H* field and vector potential *A* are related as

$$H_\theta = -\frac{1}{\mu}\frac{d\tilde{A}}{dr}. \tag{17}$$

Remembering that $\hat{n}\times\left\|\vec{H}\right\| = \vec{K}$ and the voltage linking a coil spanning one pole pitch is $2j\omega\tilde{A}$, the following relationships can be written [10]

$$\tilde{H}_1 = -\frac{\tilde{A}_1}{\mu}\frac{\gamma I_m'(\gamma a)}{I_m(\gamma a)}, \tag{18}$$

$$\begin{bmatrix}\tilde{H}_3\\ \tilde{H}_2\end{bmatrix} = \frac{1}{\mu_0}\begin{bmatrix}f_m(a,b) & g_m(b,a)\\ g_m(a,b) & f_m(b,a)\end{bmatrix}\cdot\begin{bmatrix}\tilde{A}_3\\ \tilde{A}_2\end{bmatrix}, \tag{19}$$

$$\begin{bmatrix}\tilde{H}_5\\ \tilde{H}_4\end{bmatrix} = \frac{1}{\mu_0}\begin{bmatrix}f_m(b,c) & g_m(c,b)\\ g_m(b,c) & f_m(c,b)\end{bmatrix}\cdot\begin{bmatrix}\tilde{A}_5\\ \tilde{A}_4\end{bmatrix}, \tag{20}$$

$$\tilde{H}_6 = \frac{1}{\mu_0}\frac{m}{c}\tilde{A}_6. \tag{21}$$

I_m is the modified Bessel function of the first kind, order *m*. Each $\hat{H}$ is the phasor representation of the θ component of magnetic field intensity. $\gamma = \sqrt{j\omega\mu\sigma}$ .The functions f_m and g_m are

$$f_m(x,y) = \frac{m}{y}\frac{\left[\left(\frac{x}{y}\right)^m + \left(\frac{y}{x}\right)^m\right]}{\left[\left(\frac{x}{y}\right)^m - \left(\frac{y}{x}\right)^m\right]}, \tag{22}$$

$$g_m(x,y) = \frac{2m}{x}\frac{1}{\left[\left(\frac{x}{y}\right)^m - \left(\frac{y}{x}\right)^m\right]}. \tag{23}$$

The output voltage is $V_{out} = 2j\omega\tilde{A}_3$. The input voltage depends on the resistance *R*. In terms of the surface current *K*, the equivalent current $I = K_0\int a\sin(m\theta)\,d\theta = \frac{2K_0 a}{m}$. The input voltage is

$$V_{in} = 2j\omega\tilde{A}_2 + \frac{2K_0 a}{m}R. \tag{24}$$

The vector potentials across each interface are continuous to insure $\hat{n}\cdot\left\|\vec{B}\right\| = 0$, and *H* is continuous across each interface except where the surface current lies. Solving (18) through (24) for V_{out} is

$$\frac{V_{out}}{V_{in}} = \frac{\dfrac{4m\mu^2 g_m(b,a)s\left(m\mu - c\mu_0 f_m(b,c)\right)}{\mu\mu_0}}{\left\{\begin{array}{l} 4sm\left(\begin{array}{l} f_m(c,b)\mu\mu_0 m - 4f_m(c,b)f_m(b,c)\mu_0{}^2 c - 4f_m(a,b)\mu^2 m \\ + f_m(a,b)f_m(b,c)\mu\mu_0 c + \mu_0{}^2 c g_m(c,b)g_m(b,c)\end{array}\right) \\ + f_m(c,b)aR\left(f_m(b,a)\left[\mu m - \mu_0 c\right] + \psi\left[\mu_0 m + \mu_0{}^2 c f_m(b,c)\right]\right) \\ + f_m(a,b)aR\left(\dfrac{m\mu^2}{\mu_0} + \mu c f_m(b,a) + \psi\left[a\mu m - \mu_0 c f_m(b,c)\right]\right) \\ + aRg_m(a,b)g_m(b,a)\left(m\mu^2 - \mu c f_m(b,c)\right) \\ + aRcg_m(b,c)g_m(c,b)\left(\mu_0 f_m(b,a) - \mu_0{}^2\psi\right) \end{array}\right\}} \tag{25}$$

where $\psi = \frac{\gamma I_m'(\gamma a)}{I_m(\gamma a)}$ and the Laplace transform variable has been substituted for $j\omega$.

The time constants are determined by setting the denominator of (25) to zero. At full field excitation, the equivalent relative permeability for the rotor is 26. That is, permeability μ_r=26 is that value for which the linear model reproduces the flux linkage as nonlinear analysis under full load. The principle roots of (25) for μ_r=26 is 0.28 s, in good agreement with the time harmonic results presented thus far.

IV. Power Dissipation in the Rotor

A. Emperical Approximation of Power Loss

The method is based on two papers by Yagisawa [11] [12]. Yagiwasa shows that the rotor loss per unit exposed air gap surface area is

$$\frac{P}{A} = \frac{k_m\tau^2 f^{\frac{3}{2}} B_R{}^2}{\pi^2}, \tag{26}$$

where τ is the tooth to tooth pitch span, *f* is the tooth frequency (RPM/60 · number of teeth), km is what Yagisawa called the material constant, and B_R is the magnetic field density tooth ripple. The material constant is obviously dependent on conductivity and permeability. Yagisawa measured this parameter for mild steel to be $4.2\cdot 10^5$ (W Hz$^{3/2}$ Wb^{-2}). The ripple field is that in the air gap due to the teeth.

It is implemented by analyzing the ¼ section model shown in Fig. 11. The excitations listed represent full excitation with a torque angle of 78˚. The normal B field is computed along the segment annotated in Fig. 11. The mean is subtracted and the remainder is fitted with a sin and cosine wave of the appropriate harmonic content. Let $B - \underline{B}$ represent the normal

component of B along the segment less its mean value. Assuming n teeth, the program seeks the to minimize

$$\Im = \left[\left\{B(\theta) - \underline{B}\right\} - \left\{A\cdot\cos\left(n\theta\right) + C\cdot\sin\left(n\theta\right)\right\}\right]^2 . \qquad (27)$$

B_R is $\sqrt{A^2 + C^2}$. Fig. 12 shows the normal field over the rotor pole segment, and the 18th harmonic ripple computed. Using this technique, the ripple field is computed to be 0.0502 T, and the power loss developed from (26) is 129 kW.

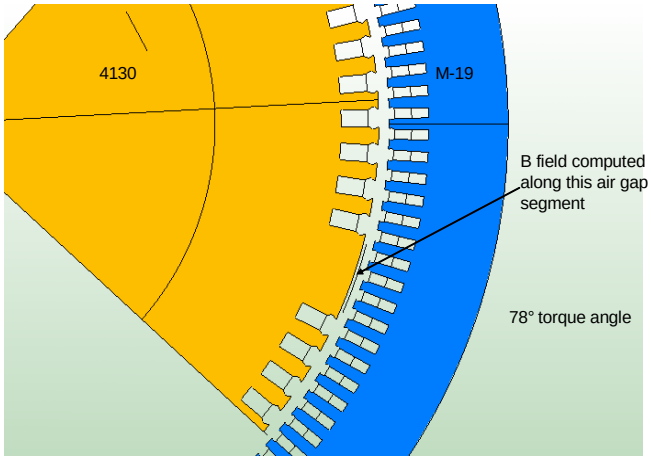

Fig. 11. Quarter section of the problem showing segment used to compute the ripple field.

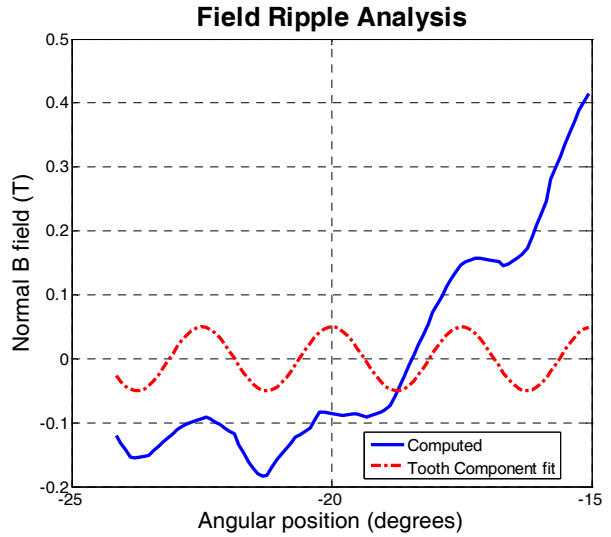

Fig. 12. Air gap field over the tooth and the equivalent curve fit for the field over the rotor tooth for only the tooth ripple harmonic.

Vector Fields rotational machines commercial transient solver was also used to compute the loss. This code treats both rotor and stator but with the standard transient vector potential equation

$$\nabla\times\left(\frac{1}{\mu}\nabla\times\vec{A}\right) = \vec{J}_S - \sigma\frac{\partial\vec{A}}{\partial t}, \qquad (28)$$

but separates the two regions by a gap that is remeshed at every time step. A layer of air elements must encapsulate the rotor, and another layer built around the stator teeth. This ensures a minimum of three elements across the air gap. The Vector Fields' solution yields a rotor loss of 108.5 kW.

B. Equivalent Surface Current Approximation of Power Loss

A novel approximation to power loss estimation involves surface current on a modified stator. Compute the tangential H field in the air gap under full load. Fourier decompose this solution to extract the tooth ripple harmonic wave number. Discard the original stator, and construct a new stator with an inner radius equal to that of the mid air gap. Set the permeability of this new stator as linear and very high (> 10^6). Place a surface current on the inner radius that approximates a sine wave with the tooth ripple wave number as suggested in Fig. 13. The boundary condition relating H and surface current K, $\hat{n}\times\left\|\vec{H}\right\| = \vec{K}$, ensures the condition that the tangential H field in the middle of the air gap reproduce that computed in the actual machine; the H field in the high permeability steel is zero. Analyze this modified stationary problem as a time harmonic eddy current problem and compute $\iint\sigma\vec{E}\cdot\vec{E}\,dS$ over the rotor. This approach is low by about 38%. It ignores contributions from other harmonics, and is only good for a rough approximation. The answer would converge only in the limit that the H field was dominated by the tooth ripple component and the fundamental, and would be closer for a non-salient rotor.

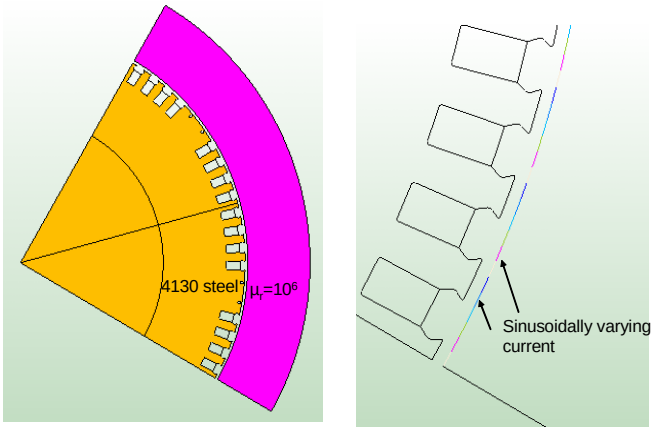

(a) Saliency removed from the stator

(b) 18th harmonic surface current on stator inner radius equal to H_t

Fig. 13. Modified generator for modeling the harmonic effect within the rotor.

V. Conclusions

Numerically modeling the transient effects of pulsed power machines can be challenging as the number of air gaps in three dimensions grows, as with macro-lamination machines. A reasonable approximation to transient performance can be obtained using a few time harmonic solutions. The complicated geometry is well modeled with a transfer function having only two poles and one zero. An analytical solution to smooth air gap machines can be formulated in terms of Bessel functions. The time constants are used in Simulink models to assess system performance.

Surface currents on a modified machine can be used to simulate a portion of the stator excitation in the air gap. The power loss induced in the solid rotor follows from a time harmonic analysis at the tooth ripple frequency. The empirical approach recommended is based on the B field over the non-salient portion of the rotor.

VI. References

[1] J. B. Schillig, H. J. Boenig, J. A. Ferner, M. K. Quissek, F. Bogdan, G. O. Linhofer, M. Eichler, G. Kasper, R. P. Marek, and J. R. Martin, "Design and testing of a 320 MW pulsed power supply," *Industry Applications Conference, 1997, Thirty-Second Industrial Applications Conference*, vol. 2, 5-9 Oct. 1997, pp. 1600-1607.

[2] J. O. Rossi, M. Ueda, V. A. Spassov, and J. J. Barroso, "A hard tube type pulse generator for plasma immersion ion implantation," *12th International Pulsed Power Conference*, vol. 2, 27-30 June 1999, pp. 1468-1471.

[3] S. B. Pratap, K. T. Hsieh, M. D. Driga, and W. F. Weldon, "Advanced compulsators for railguns," *IEEE Trans. Magn.*, vol. 25, no. 1, Jan 1989, pp 454-459.

[4] I. Smith, P. Corcoran, A. R. Miller, V. Carboni, P. Sincerny, P. Spence, C. Gilbert, W. Rix, E. Waisman, L. Schlitt, and D. Bell, "Pulse power for future and past X-ray simulators," *IEEE Trans. Plasma Sci*., vol. 30, no. 5, Oct. 2002, pp. 1746-1754.

[5] J. L. He, Z. Zabar, E. Levi, and L. Birenbaum, "Transient performance of linear induction launchers fed by generators and by capacitor banks," *IEEE Trans. Magn*., vol. 27, no. 1, Jan 1991, pp. 585-590.

[6] M. D. Driga, S. B. Pratap, A. W. Walls, and J. R. Kitzmiller, "The self-excitation process in electrical rotating machines operating in pulsed power regime," *IEEE Trans. Magn.*, vol. 37, no. 1, Jan. 2001, pp. 295-300.

[7] Kent R. Davey, "Working nonlinear transient eddy current problems with time harmonic solutions", *IEEE Trans. on Magn.*, vol. 40, no. 2, March 2004, pp. 1338-1341.

[8] T. F. Coleman and Y. Li, "An interior, trust region approach for nonlinear minimization subject to bounds," *SIAM Journal on Optimization*, vol. 6, 1996, pp. 418-445.

[9]T. F. Coleman and Y. Li, "On the convergence of reflective newton methods for large-scale nonlinear minimization subject to bounds," *Mathematical Programming*, vol. 67, no. 2, 1994, pp. 189-224.

[10] James R. Melcher, *Continuum Electromechanics*, MIT Press, Cambridge, MA, 1981, pp. 2.15-2.16, 6.12.

[11] Y. Takeda, T. Yagisawa, A. Suyama, and M. Yamamoto, "Applications of Magnetic wedges to large motors," *IEEE Trans. Magn*., vol. Mag-20, no. 5, September 1984, pp. 1780-1782.

[12] T. Yagisawa and Y. Takekoshi, *Trans. IEE Japan*, MAG 71-2, 1971.

Kent Davey (M'80-SM'86-F'04) was born in New Orleans, Louisiana, 1952. He received his BS in EE from Tulane in 1974, his MS in Power Engineering from Carnegie Mellon in 1976, and his MS in physics from the University of Pittsburgh in 1976. He received his PhD in EE from the Massachusetts Institute of Technology in 1980. He completed a Fulbright in Finland on atmospheric physics in 1981.

From 1974 to 1976 he worked at Westinghouse as a large turbine generator designer. From 1979 to 1980 he served as an assistant professor at Texas A&M University. From 1980 to 1994 he served as a tenured associate professor at the Georgia Institute of Technology. From 1994 to 2002, he served as technical director of American Maglev Technology in Edgewater, Florida. He presently serves as a research scientist at the Center for Electromechanics at the University of Texas in Austin, Texas. Dr. Davey has research activity in electromechanical machine design, pulsed electromechanical devices, HTS Trapped Field magnets, electroporation, and magnetic stimulation of biological tissue.

Dr. Davey presently serves as editor of IEEE Transactions on Magnetics. He is actively involved in the review of conference and journal papers for various IEEE activities.